Supporting information

This document contains supplemental Methods, Results, Tables and Figures. Table S1 and Figures S1-S4 are referenced directly from the main text.

1. Methods

1.1. Modeling framework

The chemistry version of the Weather Research and Forecasting (WRF-Chem) model (Skamarock *et al.*, 2008; Grell *et al.*, 2005), Advanced Research WRF (ARW) core, version 3.4.1 was used in regional simulations of meteorology and atmospheric composition including aerosol-cloud-radiation interactions. The code is publicly available through the WRF users' webpage (http://www2.mmm.ucar.edu/wrf/users/). WRF-Chem has been used extensively to characterize aerosol feedbacks in a wide variety of environments (Fast *et al.*, 2006; Chapman *et al.*, 2009; Zhao *et al.*, 2010; Zhao *et al.*, 2011; Zhao *et al.*, 2012; Gustafson *et al.*, 2007; Ntelekos *et al.*, 2009; Grell *et al.*, 2011; Saide *et al.*, 2012; Yang *et al.*, 2011; Yang *et al.*, 2012; Eidhammer *et al.*, 2014; Shrivastava *et al.*, 2013), while WRF (no chemistry) is used by many institutes for real-time experimental forecasting and also for operational numerical weather prediction (http://wrf-model.org/plots/wrfrealtime.php), and is the basis for the NOAA/NCEP Rapid Refresh and North American Mesoscale Forecast System models.

Additional WRF-Chem configuration other than the one in the main text is described as follows. The chemistry-aerosol treatment used corresponds to the CBM-Z MOSAIC (Zaveri and Peters, 1999; Zaveri *et al.*, 2008) models. MOSAIC is a sectional aerosol model and the version selected uses eight sectional size bins, two aerosol phases (dry and in-cloud), and nine aerosol composition species (aerosol water, sulfate, nitrate, ammonium, organic carbon, black carbon, sodium, chloride and other inorganics, where dust is included). It also tracks independently total aerosol number per size bin and per phase, resulting in a total of 160 aerosol and 26 gas variables tracked in the model. Other parameterization options include MYJ boundary layer (Janjić, 2002), NOAH land surface model (Chen and Dudhia, 2001), Goddard shortwave radiation (Chou *et al.*, 1998), which uses the Slingo (1989) scheme for computing cloud optical depth (COD), RRTMG longwave radiation (Mlawer *et al.*, 1997), Mie theory along with a Shell-Core mixing rule for aerosol optical properties (Fast *et al.*, 2006; Barnard *et al.*, 2010), Morrison cloud microphysics (Morrison *et al.*, 2009) and critical saturation aerosol activation (Abdul-Razzak and Ghan, 2002), with the last five options allowing the aerosol interactions with radiation and clouds (Fast *et al.*, 2006; Chapman *et al.*, 2009; Zhao *et al.*, 2011; Yang *et al.*, 2011). Modification of droplet nucleation due to aerosol composition (both from primary sources and secondary inorganic aerosols) through changes in hygroscopicity are also modeled in the activation treatment (Abdul-Razzak and Ghan, 2004). While WRF supports a variety of microphysics schemes, only two include aerosol indirect effects. Within these two we chose the Morrison scheme, which is currently among the most sophisticated and most capable of generating accurate clouds (Cintineo *et al.*, 2013). Convective parameterizations in WRF-Chem v3.4.1 do not include aerosol-cloud interactions, which is why they were not used on the outer domain. This could generate problems in the outer domain as at 12 km resolution explicit convection will not be completely resolved. However, sensitivity simulations using the Grell 3D convective parameterization (Grell and Dévényi, 2002; Grell and Freitas, 2013) on the 12 km domain did not present major changes in the smoke transport or in the smoke effects (not shown).

Although aerosol-cloud-radiation representations in models are considered to have large uncertainties (Boucher *et al.*, 2013), there seems to be a relatively greater understanding of interactions for shallow clouds (e.g., Saide *et al.*, 2012; Yang *et al.*, 2011) than for convective clouds (e.g., Ntelekos *et al.*, 2009; Eidhammer *et al.*, 2014) which could be related to the differences in extent, scale and complexity of the systems. Also, the activation parameterization used here only activates aerosols at cloud base for pre-existing clouds (Ghan *et al.*, 2001), which can be detrimental for assessing indirect effects in convective clouds, where in-cloud activation well above the base can play an important role (Pinsky and Khain, 2002). The use of a two-moment bulk microphysics scheme, compared to spectral-bin schemes, also increases uncertainties for convective cloud effects (Fan *et al.*, 2012). Thus, we expect our conclusions to be more robust when analyzing results for shallow clouds compared to convective clouds.

The accuracy of biomass burning emissions is central to quantitative skill in modeled smoke impacts. The Quick Fire Emission Dataset (QFED) v2.4 biomass burning emissions (Darmenov and da Silva, 2014) used here deals with obscured fires and employs tunable emission coefficients adjusted using an inverse modeling technique to improve model agreement with AOD estimates. This empirical fitting improves model performance. Fire emissions were coupled to the WRF-Chem online plume-rise model (Grell *et al.*, 2011). Anthropogenic emissions for the outer domain were computed using PREP-CHEM-SRC (Freitas *et al.*, 2011), and NEI 2005 was used for the inner domain (http://www.epa.gov/ttnchie1/net/2005inventory.html). Other emission sources include online MEGAN biogenics (Guenther *et al.*, 2012), Gong *et al.* (1997) sea salt parameterization and GOCART dust scheme (Zhao *et al.*, 2010). Meteorological and chemical initial and boundary conditions for the coarser domain correspond to NCEP Final Analysis (http://rda.ucar.edu/datasets/ds083.2/) and RAQMS chemical and aerosol analyses (Pierce *et al.*, 2007; Natarajan *et al.*, 2012), respectively.

Data assimilation of satellite AOD was implemented to improve modeled aerosol distributions. We used the Grid-point Statistical Interpolation (GSI) 3DVAR system (Wu *et al.*, 2002; Kleist *et al.*, 2009) modified to assimilate AOD within WRF-Chem for the MOSAIC aerosol model (Liu *et al.*, 2011; Saide *et al.*, 2013). GSI was configured similarly as previous studies (Saide *et al.*, 2013), assimilating AOD at 550 nm from the NASA NNR retrieval (GMAO, 2014) with no thinning or re-gridding, using logarithmic state and observations when minimizing the cost function, and using the NMC method (Parrish and Derber, 1992) for computing the standard deviations and vertical and horizontal length scales. As we show in the main text, transport of smoke is well represented by the model, thus, assuming that the model aerosol vertical profile is realistic and that departures from observations come mainly from differences in emissions, we used a long vertical length scale (40 vertical levels) so similar scaling factors are applied to nearly the whole column during assimilation and thus changes are distributed throughout the column. This approach is similar to 2DVAR assimilation, as is regularly done in other AOD assimilation systems (Benedetti *et al.*, 2009).

Modeled cloud top heights were computed by finding the vertical level closest to the top where cloud optical depth above it was at least 0.5. This eliminates the influence of very thin cirrus often found in the model.

2. Supporting results

2.1. Thunderstorm invigoration

Invigoration of convection by aerosols (Andreae *et al.*, 2004) is often associated with increases in precipitation (Bell *et al.*, 2008) and thunderstorm cloud top heights (Bell *et al.*, 2009). We compare these two variables for simulations Fire ON+DA and Fire OFF to investigate the possibility of convection invigoration by smoke on the April 27 outbreak. Fig S5 illustrates observed and simulated precipitation maps for the period of the outbreak with both models showing some skill in predictions of spatial patterns, with a tendency to underestimate accumulated precipitation rates. Both simulations do not represent the southern portion of the observed precipitation pattern (South-central Alabama, North-central Georgia), as no convective cells are generated in either simulation in this area. This region is excluded from the "Tornado region" of Figure S2 where tornado parameter values were assessed. By comparing the time series of precipitation and cloud heights for both simulations (Fig S5, bottom), it can be seen that the means and upper tails (75^{th} and 90^{th} percentile) of the precipitation rates and cloud heights distributions are generally higher in the simulation without smoke, with the mean differences being statistically significant most of the time. While differences in mean rain rates could be due to reduced warm rain processes by smoke effects, the upper tails of the hourly distributions are associated with convective precipitation. Thus, smoke effects start playing a role in reducing convection vigor as described in previous studies (Rosenfeld *et al.*, 2008; Koren *et al.*, 2008), which reduced precipitation and lowers cloud top heights when smoke emissions are included. However, the reduced convective vigor by smoke is only a slight effect as both simulations can fully develop updrafts (CAPE is usually over 1000 J/kg reaching values over 3000 J/kg, see Fig. S6 and S7). Thus we conclude that there is no evidence in the model that tornado occurrence or severity were enhanced by smoke invigoration of convection during this outbreak. Given the uncertainties in modeling aerosol-cloud interactions for convective cells (see section S1.1) and discrepancies compared to observed fields (e.g., lower precipitation), we cannot rule out that in reality aerosol invigoration had a role during this outbreak. However, the smoke effects described in section 3.3 of the main text are associated with shallow clouds, which we show can be responsible for the intensification of tornado parameters in the absence of a modeled aerosol invigoration effect.

2.2. Model performance for shallow clouds before the 27 April outbreak

Shallow clouds were present in both the outbreak area and the inflow region. Fig. S8 depicts satellite, in situ soundings and modeled cloud heights. GOES and MODIS have been found to overestimate low-level cloud height (Naud *et al.*, 2005). This is evident from soundings at three different locations (lower-right graph of Fig. S8) that consistently present cloud heights below 3 km. Despite this positive bias, the model seems to represent fairly well the coverage and structure of shallow clouds. Even though some of the model soundings do not indicate the multi-layer structure seen in the observations, the close proximity of the temperature and dew point at two different heights (sounding 3) suggest that this structure is present in the model in nearby grid-cells. On the other hand, modeled cloud heights are found to be biased low (from ~0 to 1 km, Fig. S8), which could be related to multiple reasons such as model vertical and horizontal resolution (e.g., Wang *et al.*, 2011), and PBL scheme for cloud layers capping the boundary layer. The model does not fully resolve the eastern side of the cloud system (over Alabama at 16:45

UTC) where broken clouds are found (Fig. S8, top panels). However, temperature and dew point differences in both the model and observations are small in this area (location #3 in Fig S8) showing that the model was close to generating local clouds.

2.3. Smoke effects on vertical profiles

As seen in Fig. S9a, the simulation including fire emissions compared to not including them presents similar wind speeds at the surface and at heights larger than 3 km, producing little change in the 0-6 km wind shear (Fig. S6). However, wind speeds around ~1 km are higher when including fire emissions, resulting in higher shear in the 0-1 km layer. The higher 0-1 km shear is due to the differences in temperature (Fig. S9b), with the simulation including fires indicating lower surface temperatures (0.65 K lower in mean, larger differences found by location, Fig. 3f), and thus presenting more stable conditions that reduce mixing and lead to sharper vertical gradients. The colder surface temperatures are due to the reduced radiation reaching the ground below optically thicker clouds and subsequent reduction in surface heat fluxes (section 3.3 main text). Also, potential temperature in the free troposphere (above 3 km) tends to be higher when smoke is included due to black carbon absorption (section 3.3 main text). As seen in Fig. S9c, water vapor is modified by two processes that happen simultaneously due to the presence of smoke. First, as surface latent heat fluxes are reduced, less evaporation occurs, reducing water vapor near the surface (Feingold *et al.*, 2005). However, this effect does not seem to play a role in the case studied as surface water vapor is not reduced by smoke effects because moisture is mainly transported from the GoM (Knupp *et al.*, 2013). Second, the smoke stabilization reduces entrainment of dry air, maintaining moisture in the mixed layer and increasing water vapor near the top of the mixed layer

(Brioude *et al.*, 2009; Wilcox, 2010). Overall, there is a general increase in relative humidity in the mixed layer when smoke is present (Fig. S9d), due to the moisture accumulation and the lower temperatures at the surface. The higher relative humidity and more stable conditions under the presence of smoke produce lower cloud base and LCL. CAPE is only slightly modified by the presence of smoke (Fig. S6) due to compensating effects of the changes in temperature in multiple levels and water vapor profiles.

References

Abdul-Razzak, H., and Ghan, S. J.: A parameterization of aerosol activation 3. Sectional representation, J. Geophys. Res., 107, 4026, 10.1029/2001jd000483, 2002.

Abdul-Razzak, H., and Ghan, S. J.: Parameterization of the influence of organic surfactants on aerosol activation, Journal of Geophysical Research: Atmospheres, 109, D03205, 10.1029/2003jd004043, 2004.

Andreae, M. O., Rosenfeld, D., Artaxo, P., Costa, A. A., Frank, G. P., Longo, K. M., and Silva-Dias, M. A. F.: Smoking Rain Clouds over the Amazon, Science, 303, 1337-1342, 10.1126/science.1092779, 2004.

Barnard, J. C., Fast, J. D., Paredes-Miranda, G., Arnott, W. P., and Laskin, A.: Technical Note: Evaluation of the WRF-Chem "Aerosol Chemical to Aerosol Optical Properties" Module using data from the MILAGRO campaign, Atmos. Chem. Phys., 10, 7325-7340, 10.5194/acp-10-7325-2010, 2010.

Bell, T. L., Rosenfeld, D., Kim, K.-M., Yoo, J.-M., Lee, M.-I., and Hahnenberger, M.: Midweek increase in U.S. summer rain and storm heights suggests air pollution invigorates rainstorms, Journal of Geophysical Research: Atmospheres, 113, D02209, 10.1029/2007jd008623, 2008.

Bell, T. L., Yoo, J.-M., and Lee, M.-I.: Note on the weekly cycle of storm heights over the southeast United States, Journal of Geophysical Research: Atmospheres, 114, D15201, 10.1029/2009jd012041, 2009.

Benedetti, A., Morcrette, J., Boucher, O., Dethof, A., Engelen, R., Fisher, M., Flentje, H., Huneeus, N., Jones, L., and Kaiser, J.: Aerosol analysis and forecast in the European Centre for Medium-Range Weather Forecasts Integrated Forecast System: 2. Data assimilation, J. Geophys. Res, 114, D13205, 2009.

Boucher, O., Randall, D., Artaxo, P., Bretherton, C., Feingold, G., Forster, P., Kerminen, V.-M., Kondo, Y., Liao, H., Lohmann, U., Rasch, P., Satheesh, S. K., Sherwood, S., Stevens, B., and Zhang, X. Y.: Clouds and Aerosols. In: Climate Change 2013: The

Physical Science Basis. Contribution of Working Group I to the Fifth Assessment Report of the Intergovernmental 25 Panel on Climate Change, edited by: Stocker, T. F., Qin, D., Plattner, G.-K., Tignor, M., Allen, S. K., Boschung, J., Nauels, A., Xia, Y., Bex, V., and Midgley, P. M.,, Cambridge University Press, Cambridge, United Kingdom and New York, NY, USA,, 2013.

Brioude, J., Cooper, O. R., Feingold, G., Trainer, M., Freitas, S. R., Kowal, D., Ayers, J. K., Prins, E., Minnis, P., McKeen, S. A., Frost, G. J., and Hsie, E. Y.: Effect of biomass burning on marine stratocumulus clouds off the California coast, Atmos. Chem. Phys., 9, 8841-8856, 10.5194/acp-9-8841-2009, 2009.

Chapman, E., Gustafson Jr, W., Easter, R., Barnard, J., Ghan, S., Pekour, M., and Fast, J.: Coupling aerosol-cloud-radiative processes in the WRF-Chem model: Investigating the radiative impact of elevated point sources, Atmos. Chem. Phys., 9, 945-964, 2009.

Chen, F., and Dudhia, J.: Coupling an advanced land surface-hydrology model with the Penn State-NCAR MM5 modeling system. Part I: Model implementation and sensitivity, Monthly Weather Review, 129, 569-585, 2001.

Chou, M.-D., Suarez, M. J., Ho, C.-H., Yan, M. M., and Lee, K.-T.: Parameterizations for cloud overlapping and shortwave single-scattering properties for use in general circulation and cloud ensemble models, Journal of climate, 11, 202-214, 1998.

Cintineo, R., Otkin, J. A., Xue, M., and Kong, F.: Evaluating the Performance of Planetary Boundary Layer and Cloud Microphysical Parameterization Schemes in Convection-Permitting Ensemble Forecasts using Synthetic GOES-13 Satellite Observations, Monthly Weather Review, Under review, 2013.

Darmenov, A., and da Silva, A. M.: The Quick Fire Emissions Dataset (QFED) - Documentation of versions 2.1, 2.2 and 2.4, NASA TM-2013-104606, Vol. 35, (http://gmao.gsfc.nasa.gov/pubs/tm/), 183 pp, 2014.

Diamond, H. J., Karl, T. R., Palecki, M. A., Baker, C. B., Bell, J. E., Leeper, R. D., Easterling, D. R., Lawrimore, J. H., Meyers, T. P., Helfert, M. R., Goodge, G., and Thorne, P. W.: U.S. Climate Reference Network after One Decade of Operations: Status and Assessment, Bulletin of the American Meteorological Society, 94, 485-498, 10.1175/bams-d-12-00170.1, 2013.

Dubovik, O., and King, M. D.: A flexible inversion algorithm for retrieval of aerosol optical properties from Sun and sky radiance measurements, Journal of Geophysical Research: Atmospheres, 105, 20673-20696, 10.1029/2000jd900282, 2000.

Eidhammer, T., Barth, M. C., Petters, M. D., Wiedinmyer, C., and Prenni, A. J.: Aerosol microphysical impact on summertime convective precipitation in the Rocky Mountain region, Journal of Geophysical Research: Atmospheres, 2014JD021883, 10.1002/2014jd021883, 2014.

EPA: http://www.epa.gov/ttn/airs/airsaqs/, 2013.

Fan, J., Leung, L. R., Li, Z., Morrison, H., Chen, H., Zhou, Y., Qian, Y., and Wang, Y.: Aerosol impacts on clouds and precipitation in eastern China: Results from bin and bulk microphysics, Journal of Geophysical Research: Atmospheres, 117, D00K36, 10.1029/2011jd016537, 2012.

Fast, J. D., Gustafson Jr, W. I., Easter, R. C., Zaveri, R. A., Barnard, J. C., Chapman, E. G., Grell, G. A., and Peckham, S. E.: Evolution of ozone, particulates, and aerosol direct radiative forcing in the vicinity of Houston using a fully coupled meteorology-chemistry-aerosol model, Journal of Geophysical Research, 111, D21305, 2006.

Feingold, G., Jiang, H., and Harrington, J. Y.: On smoke suppression of clouds in Amazonia, Geophys. Res. Lett., 32, L02804, 10.1029/2004gl021369, 2005.

Freitas, S. R., Longo, K. M., Alonso, M. F., Pirre, M., Marecal, V., Grell, G., Stockler, R., Mello, R. F., and Sánchez Gácita, M.: PREP-CHEM-SRC – 1.0: a preprocessor of trace gas and aerosol emission fields for regional and global atmospheric chemistry models, Geosci. Model Dev., 4, 419-433, 10.5194/gmd-4-419-2011, 2011.

Ghan, S., Easter, R., Hudson, J., and Bréon, F.-M.: Evaluation of aerosol indirect radiative forcing in MIRAGE, Journal of Geophysical Research: Atmospheres, 106, 5317-5334, 10.1029/2000jd900501, 2001.

GMAO: http://gmao.gsfc.nasa.gov/forecasts/, 2014.

Gong, S., Barrie, L., and Blanchet, J.-P.: Modeling sea-salt aerosols in the atmosphere 1. Model development, Journal of Geophysical Research, 102, 3805-3818, 1997.

Grell, G., Peckham, S. E., Schmitz, R., McKeen, S. A., Frost, G., Skamarock, W. C., and Eder, B.: Fully coupled "online" chemistry within the WRF model, Atmos. Environ., 39, 6957-6975, 10.1016/j.atmosenv.2005.04.027, 2005.

Grell, G., Freitas, S. R., Stuefer, M., and Fast, J.: Inclusion of biomass burning in WRF-Chem: impact of wildfires on weather forecasts, Atmos. Chem. Phys., 11, 5289-5303, 10.5194/acp-11-5289-2011, 2011.

Grell, G. A., and Dévényi, D.: A generalized approach to parameterizing convection combining ensemble and data assimilation techniques, Geophys. Res. Lett., 29, 38-31-38-34, 10.1029/2002gl015311, 2002.

Grell, G. A., and Freitas, S. R.: A scale and aerosol aware stochastic convective parameterization for weather and air quality modeling, Atmos. Chem. Phys. Discuss., 13, 23845-23893, 10.5194/acpd-13-23845-2013, 2013.

Guenther, A. B., Jiang, X., Heald, C. L., Sakulyanontvittaya, T., Duhl, T., Emmons, L. K., and Wang, X.: The Model of Emissions of Gases and Aerosols from Nature version 2.1 (MEGAN2.1): an extended and updated framework for modeling biogenic emissions, Geosci. Model Dev., 5, 1471-1492, 10.5194/gmd-5-1471-2012, 2012.

Gustafson, W. I., Chapman, E. G., Ghan, S. J., Easter, R. C., and Fast, J. D.: Impact on modeled cloud characteristics due to simplified treatment of uniform cloud condensation nuclei during NEAQS 2004, Geophys. Res. Lett., 34, L19809, 10.1029/2007gl030021, 2007.

Janjić, Z. I.: Nonsingular implementation of the Mellor–Yamada level 2.5 scheme in the NCEP Meso model, NCEP office note, 437, 61, 2002.

King, M. D., Platnick, S., Hubanks, P. A., Arnold, G. T., Moody, E. G., Wind, G., and Wind, B.: Collection 005 change summary for the MODIS cloud optical property (06_OD) algorithm, Available: modis-atmos. gsfc. nasa. gov/C005_Changes/C005_ CloudOpticalProperties_ver311. pdf, 2006.

Kleist, D. T., Parrish, D. F., Derber, J. C., Treadon, R., Wu, W.-S., and Lord, S.: Introduction of the GSI into the NCEP global data assimilation system, Weather and Forecasting, 24, 1691-1705, 2009.

Knupp, K. R., Murphy, T. A., Coleman, T. A., Wade, R. A., Mullins, S. A., Schultz, C. J., Schultz, E. V., Carey, L., Sherrer, A., McCaul, E. W., Carcione, B., Latimer, S., Kula, A., Laws, K., Marsh, P. T., and Klockow, K.: Meteorological Overview of the Devastating 27 April 2011 Tornado Outbreak, Bulletin of the American Meteorological Society, 95, 1041-1062, 10.1175/bams-d-11-00229.1, 2013.

Koren, I., Martins, J. V., Remer, L. A., and Afargan, H.: Smoke invigoration versus inhibition of clouds over the Amazon, Science, 321, 946, 2008.

Lin, Y., and Mitchell, K. E.: The NCEP Stage II/IV hourly precipitation analyses: development and applications, Preprints, 19th Conf. on Hydrology, American Meteorological Society, San Diego, CA, 9-13 January 2005, Paper 1.2., 2005.

Liu, Z., Liu, Q., Lin, H. C., Schwartz, C. S., Lee, Y. H., and Wang, T.: Three-dimensional variational assimilation of MODIS aerosol optical depth: Implementation and application to a dust storm over East Asia, Journal of Geophysical Research, 116, D23206, 2011.

Mlawer, E. J., Taubman, S. J., Brown, P. D., Iacono, M. J., and Clough, S. A.: Radiative transfer for inhomogeneous atmospheres: RRTM, a validated correlated-k model for the longwave, Journal of Geophysical Research: Atmospheres, 102, 16663-16682, 10.1029/97jd00237, 1997.

Morrison, H., Thompson, G., and Tatarskii, V.: Impact of Cloud Microphysics on the Development of Trailing Stratiform Precipitation in a Simulated Squall Line: Comparison of One- and Two-Moment Schemes, Monthly Weather Review, 137, 991-1007, 10.1175/2008mwr2556.1, 2009.

Nakanishi, M., and Niino, H.: An improved Mellor–Yamada level-3 model with condensation physics: Its design and verification, Boundary-layer meteorology, 112, 1-31, 2004.

Natarajan, M., Pierce, R. B., Schaack, T. K., Lenzen, A. J., Al-Saadi, J. A., Soja, A. J., Charlock, T. P., Rose, F. G., Winker, D. M., and Worden, J. R.: Radiative forcing due to enhancements in tropospheric ozone and carbonaceous aerosols caused by Asian fires during spring 2008, Journal of Geophysical Research: Atmospheres, 117, D06307, 10.1029/2011jd016584, 2012.

Naud, C. M., Muller, J. P., Clothiaux, E. E., Baum, B. A., and Menzel, W. P.: Intercomparison of multiple years of MODIS, MISR and radar cloud-top heights, Ann. Geophys., 23, 2415-2424, 10.5194/angeo-23-2415-2005, 2005.

NOAA NWS: http://www.ua.nws.noaa.gov/, 2013.

Ntelekos, A. A., Smith, J. A., Donner, L., Fast, J. D., Gustafson, W. I., Chapman, E. G., and Krajewski, W. F.: The effects of aerosols on intense convective precipitation in the northeastern United States, Quarterly Journal of the Royal Meteorological Society, 135, 1367-1391, 10.1002/qj.476, 2009.

O'Neill, N. T., Eck, T. F., Smirnov, A., Holben, B. N., and Thulasiraman, S.: Spectral discrimination of coarse and fine mode optical depth, Journal of Geophysical Research: Atmospheres, 108, 4559, 10.1029/2002jd002975, 2003.

Parrish, D. F., and Derber, J. C.: The National Meteorological Center's spectral statistical-interpolation analysis system, Monthly Weather Review, 120, 1747-1763, 1992.

Pavolonis, M. J., Heidinger, A. K., and Uttal, T.: Daytime Global Cloud Typing from AVHRR and VIIRS: Algorithm Description, Validation, and Comparisons, Journal of Applied Meteorology, 44, 804-826, 10.1175/jam2236.1, 2005.

Pierce, R. B., Schaack, T., Al-Saadi, J. A., Fairlie, T. D., Kittaka, C., Lingenfelser, G., Natarajan, M., Olson, J., Soja, A., Zapotocny, T., Lenzen, A., Stobie, J., Johnson, D., Avery, M. A., Sachse, G. W., Thompson, A., Cohen, R., Dibb, J. E., Crawford, J., Rault, D., Martin, R., Szykman, J., and Fishman, J.: Chemical data assimilation estimates of continental U.S. ozone and nitrogen budgets during the Intercontinental Chemical Transport Experiment–North America, Journal of Geophysical Research: Atmospheres, 112, D12S21, 10.1029/2006jd007722, 2007.

Pinsky, M. B., and Khain, A. P.: Effects of in-cloud nucleation and turbulence on droplet spectrum formation in cumulus clouds, Quarterly Journal of the Royal Meteorological Society, 128, 501-533, 10.1256/003590002321042072, 2002.

Platnick, S., King, M. D., Ackerman, S. A., Menzel, W. P., Baum, B. A., Riedi, J. C., and Frey, R. A.: The MODIS cloud products: algorithms and examples from Terra, Geoscience and Remote Sensing, IEEE Transactions on, 41, 459-473, 10.1109/tgrs.2002.808301, 2003.

Potter, S.: Fine-Tuning Fujita: After 35 years, a new scale for rating tornadoes takes effect, Weatherwise, 60, 64-71, 10.3200/wewi.60.2.64-71, 2007.

Rosenfeld, D., Lohmann, U., Raga, G. B., O'Dowd, C. D., Kulmala, M., Fuzzi, S., Reissell, A., and Andreae, M. O.: Flood or Drought: How Do Aerosols Affect Precipitation?, Science, 321, 1309-1313, 10.1126/science.1160606, 2008.

Saide, P. E., Spak, S. N., Carmichael, G. R., Mena-Carrasco, M. A., Yang, Q., Howell, S., Leon, D. C., Snider, J. R., Bandy, A. R., Collett, J. L., Benedict, K. B., de Szoeke, S. P., Hawkins, L. N., Allen, G., Crawford, I., Crosier, J., and Springston, S. R.: Evaluating WRF-Chem aerosol indirect effects in Southeast Pacific marine stratocumulus during VOCALS-REx, Atmos. Chem. Phys., 12, 3045-3064, 10.5194/acp-12-3045-2012, 2012.

Saide, P. E., Carmichael, G. R., Liu, Z., Schwartz, C. S., Lin, H. C., da Silva, A. M., and Hyer, E.: Aerosol optical depth assimilation for a size-resolved sectional model: impacts of observationally constrained, multi-wavelength and fine mode retrievals on regional scale analyses and forecasts, Atmos. Chem. Phys., 13, 10425-10444, 10.5194/acp-13-10425-2013, 2013.

Shrivastava, M., Berg, L. K., Fast, J. D., Easter, R. C., Laskin, A., Chapman, E. G., Gustafson, W. I., Liu, Y., and Berkowitz, C. M.: Modeling aerosols and their interactions with shallow cumuli during the 2007 CHAPS field study, Journal of Geophysical Research: Atmospheres, 118, 1343-1360, 10.1029/2012jd018218, 2013.

Skamarock, W. C., Klemp, J. B., Dudhia, J., Gill, D. O., Barker, D. M., Duda, M. G., Huang, X.-Y., Wang, W., and Powers, J. G.: A description of the Advanced Research WRF version 3, NCAR Tech. Note NCAR/TN-475+ STR, 2008.

Slingo, A.: A GCM Parameterization for the Shortwave Radiative Properties of Water Clouds, Journal of the atmospheric sciences, 46, 1419-1427, 10.1175/1520-0469(1989)046<1419:agpfts>2.0.co;2, 1989.

SPC: Tornado, Hail, and Wind Database available online at SPC WCM web page (http://www.spc.noaa.gov/wcm/#data), 2013.

Wang, S., O'Neill, L. W., Jiang, Q., de Szoeke, S. P., Hong, X., Jin, H., Thompson, W. T., and Zheng, X.: A regional real-time forecast of marine boundary layers during VOCALS-REx, Atmos. Chem. Phys., 11, 421-437, 10.5194/acp-11-421-2011, 2011.

Wilcox, E. M.: Stratocumulus cloud thickening beneath layers of absorbing smoke aerosol, Atmos. Chem. Phys., 10, 11769-11777, 10.5194/acp-10-11769-2010, 2010.

Wu, W.-S., Purser, R. J., and Parrish, D. F.: Three-dimensional variational analysis with spatially inhomogeneous covariances, Monthly Weather Review, 130, 2905-2916, 2002.

Yang, Q., W. I. Gustafson, J., Fast, J. D., Wang, H., Easter, R. C., Morrison, H., Lee, Y. N., Chapman, E. G., Spak, S. N., and Mena-Carrasco, M. A.: Assessing regional scale predictions of aerosols, marine stratocumulus, and their interactions during VOCALS-REx using WRF-Chem, Atmos. Chem. Phys., 11, 11951-11975, 10.5194/acp-11-11951-2011, 2011.

Yang, Q., Gustafson Jr, W. I., Fast, J. D., Wang, H., Easter, R. C., Wang, M., Ghan, S. J., Berg, L. K., Leung, L. R., and Morrison, H.: Impact of natural and anthropogenic aerosols on stratocumulus and precipitation in the Southeast Pacific: a regional modelling study using WRF-Chem, Atmos. Chem. Phys., 12, 8777-8796, 10.5194/acp-12-8777-2012, 2012.

Young, S. A., and Vaughan, M. A.: The Retrieval of Profiles of Particulate Extinction from Cloud-Aerosol Lidar Infrared Pathfinder Satellite Observations (CALIPSO) Data: Algorithm Description, Journal of Atmospheric and Oceanic Technology, 26, 1105-1119, 10.1175/2008jtecha1221.1, 2009.

Zaveri, R. A., and Peters, L. K.: A new lumped structure photochemical mechanism for large-scale applications, Journal of Geophysical Research, 104, 30387-30330,30415, 1999.

Zaveri, R. A., Easter, R. C., Fast, J. D., and Peters, L. K.: Model for simulating aerosol interactions and chemistry (MOSAIC), J. Geophys. Res, 113, D13204, 2008.

Zhao, C., Liu, X., Leung, L. R., Johnson, B., McFarlane, S. A., Gustafson Jr, W. I., Fast, J. D., and Easter, R.: The spatial distribution of mineral dust and its shortwave radiative forcing over North Africa: modeling sensitivities to dust emissions and aerosol size treatments, Atmos. Chem. Phys., 10, 8821-8838, 10.5194/acp-10-8821-2010, 2010.

Zhao, C., Liu, X., Ruby Leung, L., and Hagos, S.: Radiative impact of mineral dust on monsoon precipitation variability over West Africa, Atmos. Chem. Phys., 11, 1879-1893, 10.5194/acp-11-1879-2011, 2011.

Zhao, C., Liu, X., and Leung, L. R.: Impact of the Desert dust on the summer monsoon system over Southwestern North America, Atmos. Chem. Phys., 12, 3717-3731, 10.5194/acp-12-3717-2012, 2012.

Supporting Tables

Table S1: Observational data used in the study. COD: Cloud optical Depth, LWP: Liquid Water Path, AOD: Aerosol Optical Depth, PM2.5: aerosol mass of sizes below 2.5 μm, AERONET: Aerosol RObotic NETwork, GOES13: Geostationary Operational Environmental Satellites number 13, CALIPSO: Cloud-Aerosol Lidar and Infrared Pathfinder Satellite Observations, AQS: Air Quality System, NEXRAD: Next-Generation Radar, USRCRN: U.S. Regional Climate Reference Network, SPC: Storm Prediction Center, MODIS: Moderate Resolution Imaging Spectroradiometer, CALIOP: Cloud-Aerosol Lidar with Orthogonal Polarization, NNR: Neural Network Retrieval, SDA: Spectral Deconvolution Algorithm. The following data is available through the websites in parenthesis: MODIS (http://ladsweb.nascom.nasa.gov/data/search.html), AERONET (http://aeronet.gsfc.nasa.gov/), CALIPSO (http://reverb.echo.nasa.gov/), AQS (www.epa.gov/rsig/), Rainfall (http://data.eol.ucar.edu/codiac/dss/id=21.093), USRCRN and tornado tracks (http://www.ncdc.noaa.gov/), Upper air soundings (http://weather.uwyo.edu/upperair/sounding.html)

Observation	Satellite / Network	Instrument	Algorithm	Reference
COD	Terra/Aqua	MODIS	-	(King *et al.*, 2006)
	GOES 13	Imager	PATMOS-x	(Pavolonis *et al.*, 2005)
Cloud top heights	GOES 13	Imager	PATMOS-x	(Pavolonis *et al.*, 2005)
	Terra/Aqua	MODIS	Use WRF-Chem pressure levels to obtain height	(Platnick *et al.*, 2003)
AOD	Terra/Aqua	MODIS	NASA NNR	(GMAO, 2014)
	AERONET	Sun photometer	SDA	(O'Neill *et al.*, 2003)
Angstrom Exponent	AERONET	Sun photometer	AOD	(Dubovik and King, 2000)
Aerosol plume	CALIPSO	CALIOP	Feature type	(Young and Vaughan,

height			detection	2009)
Ground PM2.5	AQS	TEOMS, FRM	-	(EPA, 2013)
Rainfall	NEXRAD + rain gauges	Radar and rain gauges	Stage IV	(Lin and Mitchell, 2005)
Solar radiation	USRCRN	Pyranometer	-	(Diamond *et al.*, 2013)
Cloud height	Upper air	Radiosonde	-	(NOAA NWS, 2013)
Tornado tracks	SPC	-	Reports and damage surveys	(SPC, 2013)

Supporting Figures

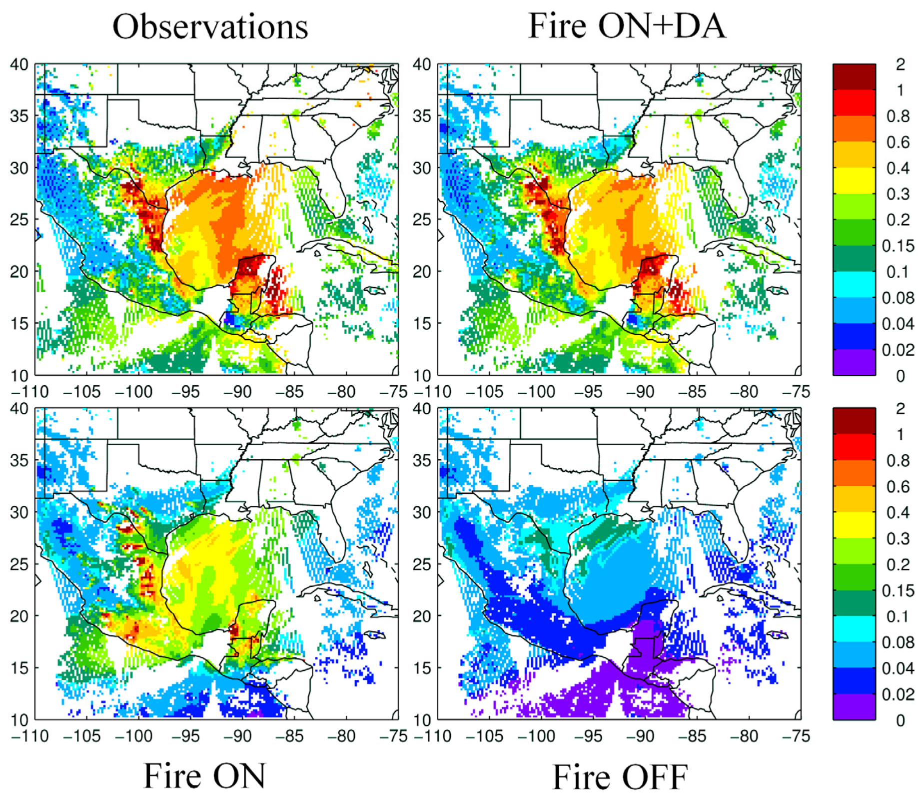

Figure S1. Average NASA NNR AOD (top-left) and model estimates maps for Terra and Aqua on 27 April. Simulations correspond to including fire emissions and data assimilation (top-right), fire emissions with no data assimilation (bottom-left) and not including fire emissions (bottom-right).

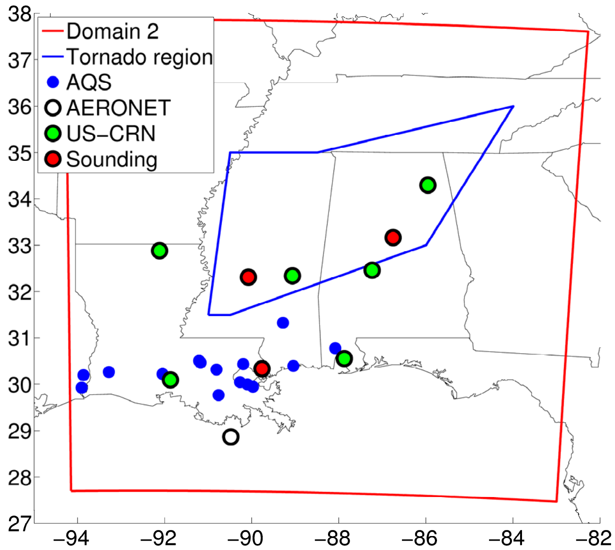

Figure S2. Inner modeling domain, analysis region, and observational networks. See definitions on Table S1 and outer domain in Fig. 1.

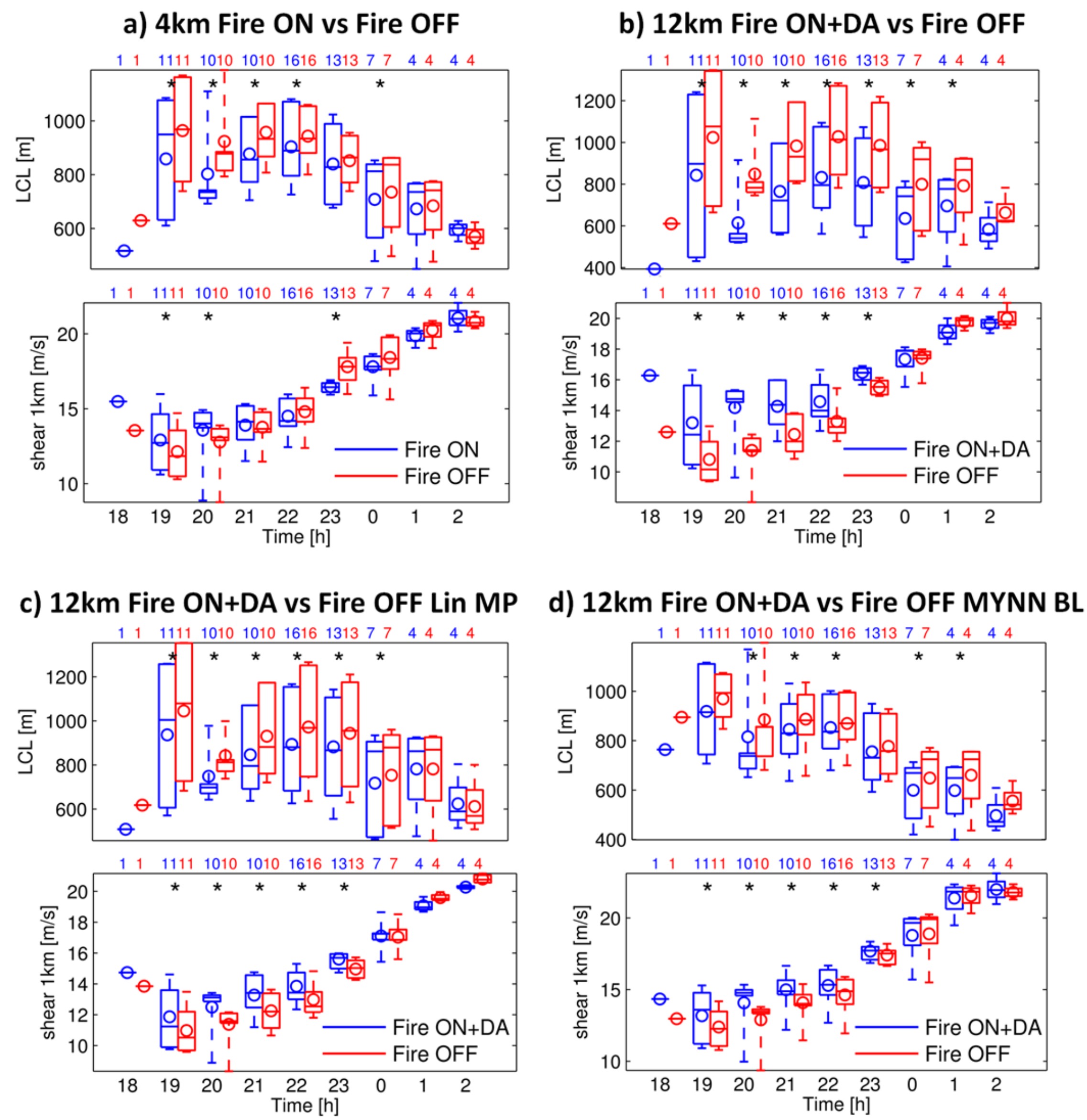

Figure S3. As Fig. 2 but for LCL and 1 km shear. The panels show **a)** Fire ON (no data assimilation) and Fire OFF simulations at 4 km resolution using the base model configuration, **b)** Fire ON+DA and Fire OFF simulations at 12 km resolution using the base model configuration, **c)** Fire ON+DA and Fire OFF simulations at 12 km resolution but using the Lin microphysics scheme (Chapman *et al.*, 2009) and **d)** Fire ON+DA and Fire OFF simulations at 12 km resolution but using the MYNN boundary layer scheme (Nakanishi and Niino, 2004).

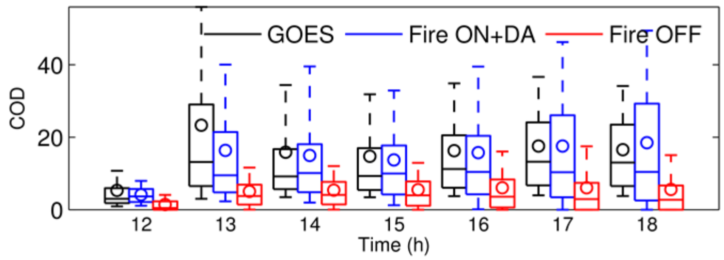

Figure S4. Cloud optical depth statistics as in Fig. 2 for GOES13 and models over the inflow region (Fig. 3) before the outbreak.

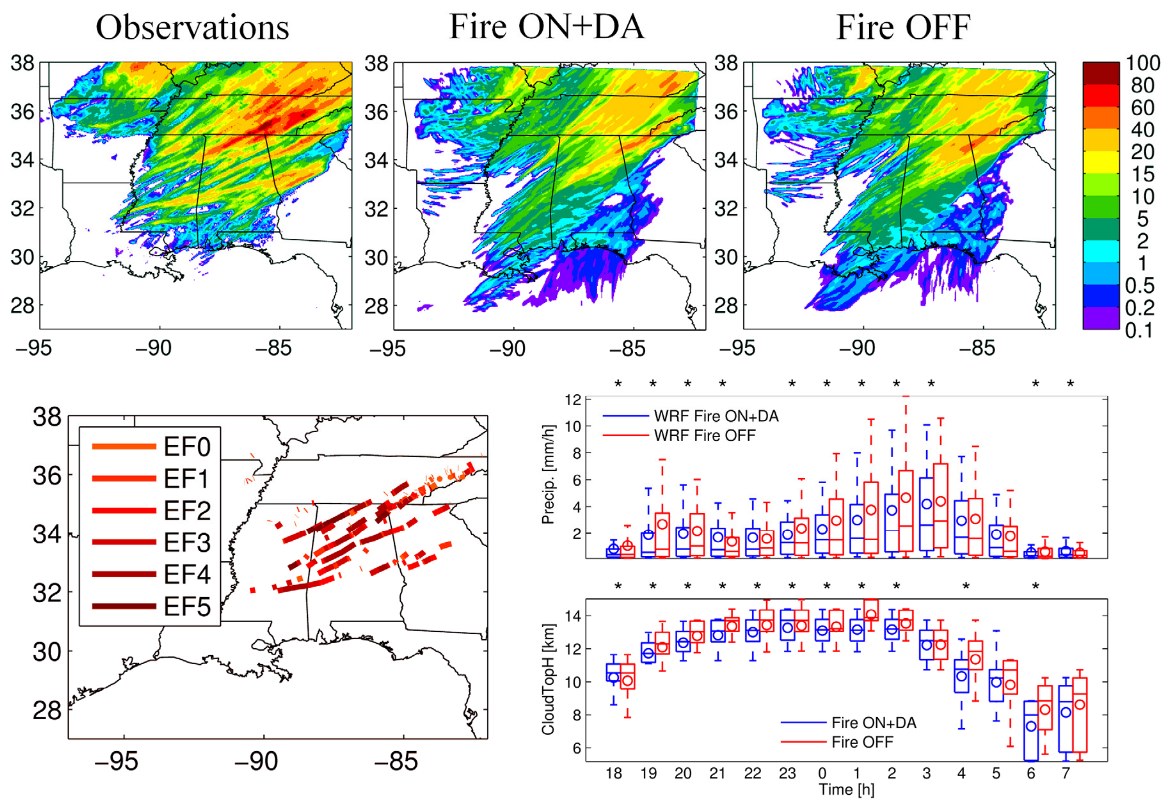

Figure S5. Top panels: Observed and model twelve hour accumulated precipitation (mm) valid at 6 UTC on 28 April. Bottom-left: Tornado tracks color coded by magnitude on the Enhanced Fujita (EF) Scale (Potter, 2007). Bottom-right panels: Model statistics as in Fig. 2 for precipitation and cloud top height for the "Tornado region" depicted in Fig S2. Precipitation over 0.1 mm/h and cloud top heights over 5 km were considered when computing statistics. Statistically significance differences for each time are represented by the symbol "*" on top of each panel.

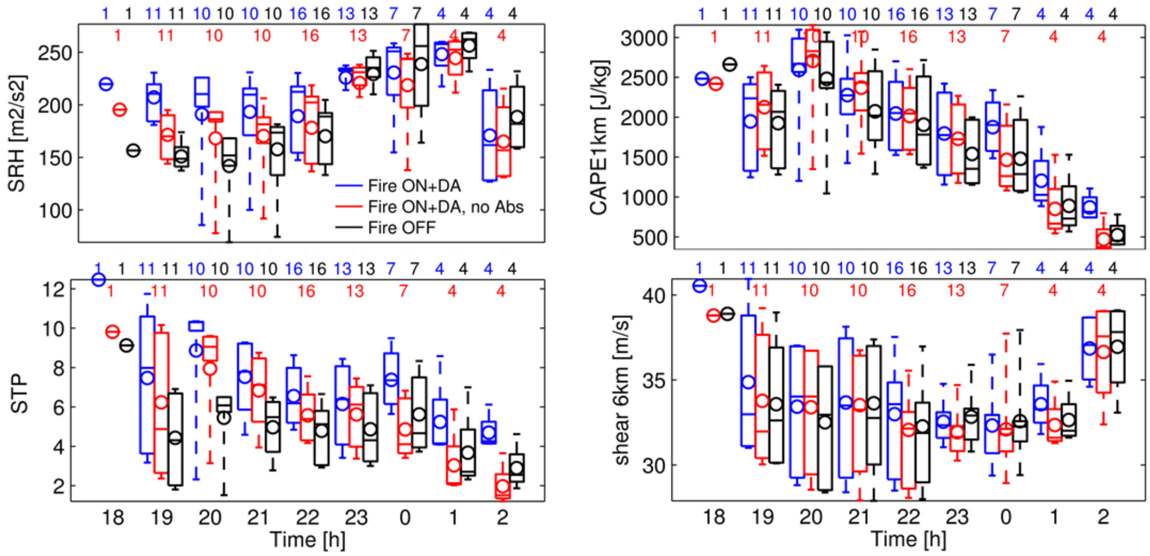

Figure S6. Hourly box and whisker distributions as in Fig. 2 of model parameters used in tornado forecasting. The three models represent simulations with fire emissions and data assimilation (Fire ON+DA), fire emissions and data assimilation with black carbon absorption set to 0 (Fire ON+DA, no Abs), and no fire emissions (Fire OFF). Statistics are computed as in Fig 2.

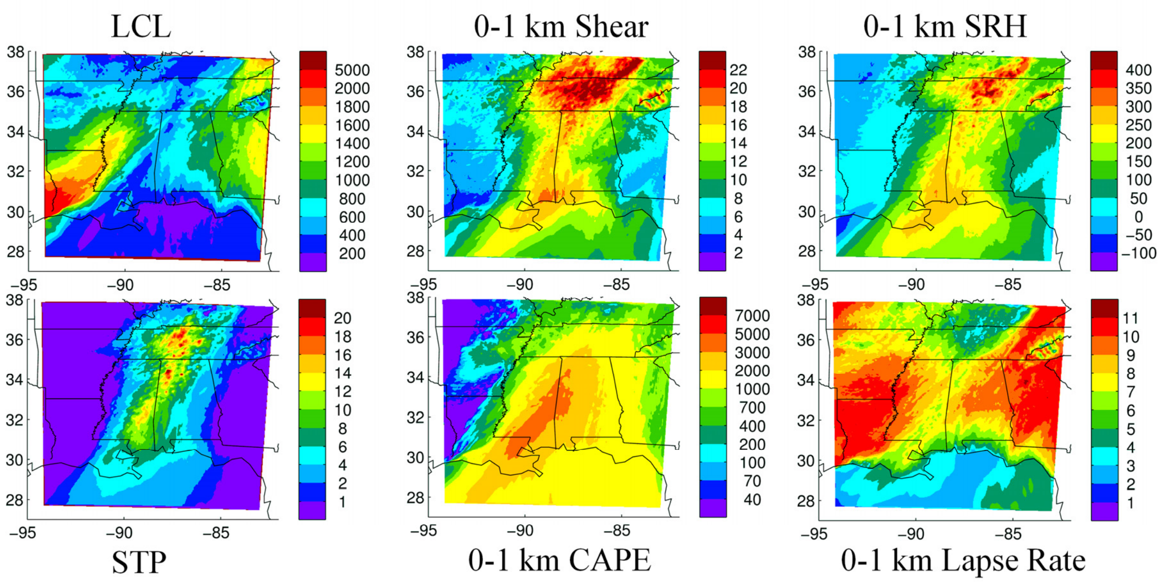

Figure S7. Maps of selected parameters averaged from 18 to 00 UTC for the simulation using fire emissions and data assimilation. Units: LCL in m, shear in m/s, CAPE in J/kg SRH in m^2/s^2 and Lapse Rate in C/km.

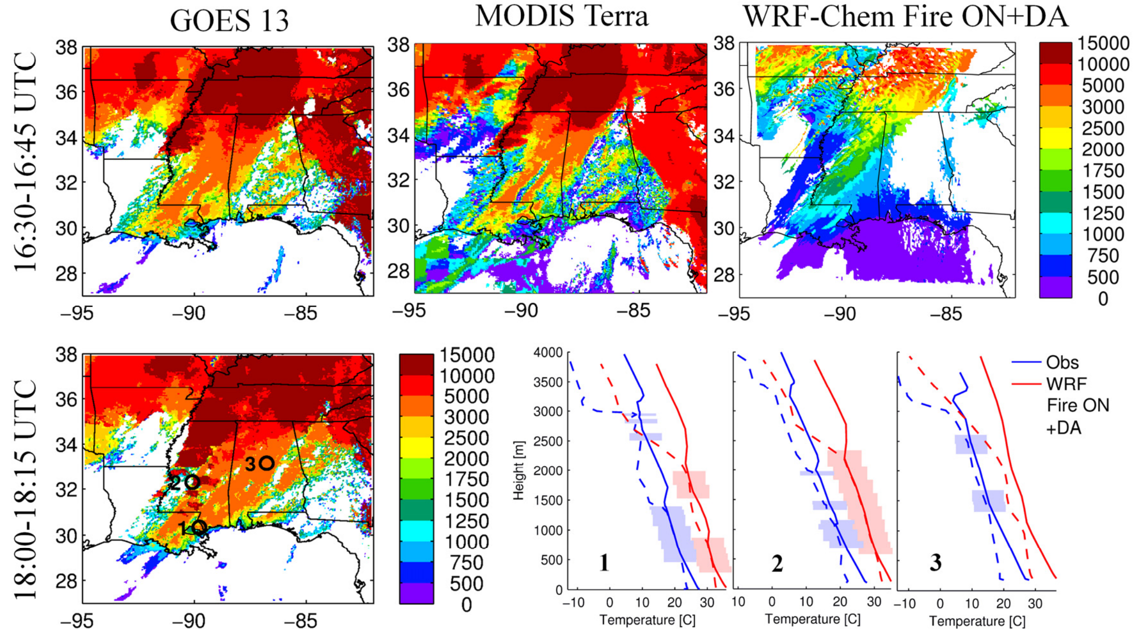

Figure S8. Top and bottom-left panels: Cloud top height (in m) maps for 27 April. Upper row illustrates GOES13, MODIS and WRF-Chem model (with fire emissions and data assimilation) for 16:30-16:45 UTC (Terra overpass at 16:30, GOES scan at 16:45), while the bottom panel shows GOES13 at 18:15 UTC. Bottom right panels: Temperature (T, solid lines) and dew point temperature (Td, dashed lines) profiles for three special upper air soundings (location indicated on bottom-left map) and model at 18 UTC. Model profiles are shifted +10 C to avoid overlapping and to improve visualization. Blue shading indicates T and Td difference of less than 1.5 ºC, which suggests overcast or broken cloud conditions, while red shading represents model cloud occurrence.

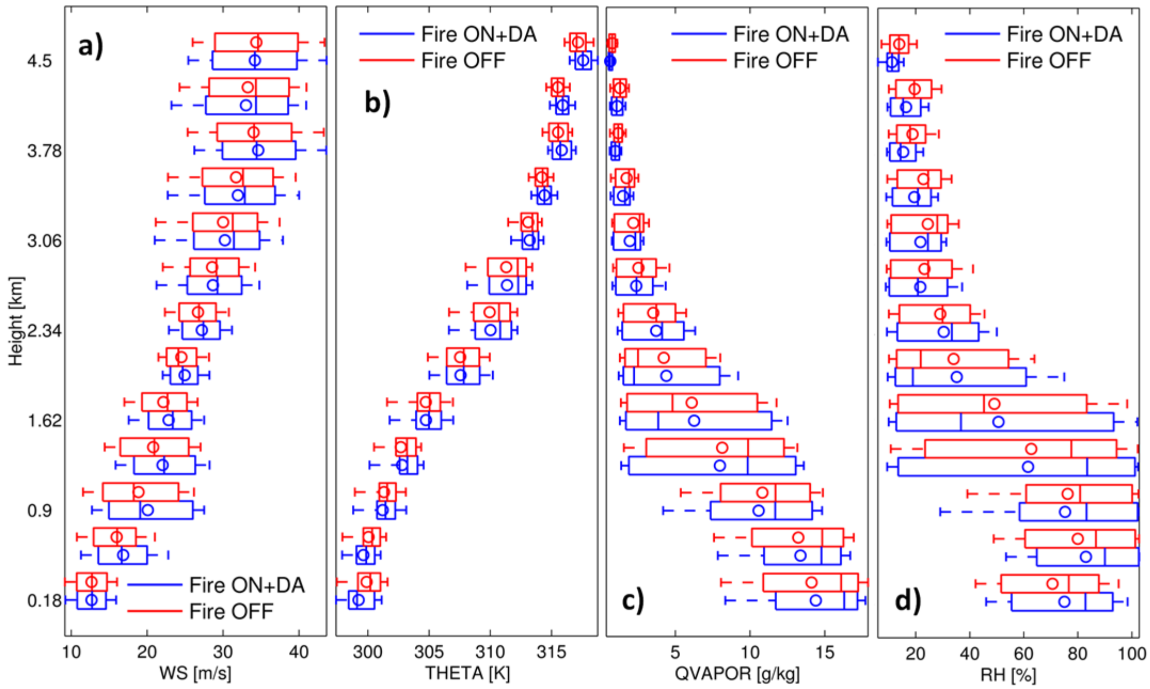

Figure S9. Statistics as in Fig. 2 for vertical profiles at 16 UTC over the inflow region (Fig. 3) for simulations with fire emissions and data assimilation and without fire emissions. Box and whisker plots are shown for wind speed (WS, **a**), potential temperature (THETA, **b**), water vapor (QVAPOR, **c**) and relative humidity (RH, **d**).